Electronic properties, low-energy Hamiltonian, and superconducting instabilities in $CaKFe_4As_4$

Felix Lochner,[1,2] Felix Ahn,[2] Tilmann Hickel,[1] and Ilya Eremin[2,3]
[1]*Max-Planck-Institut für Eisenforschung, D-40237 Düsseldorf, Germany*
[2]*Institut für Theoretische Physic III, Ruhr-Universität Bochum, D-44801 Bochum, Germany*
[3]*National University of Science and Technology "MISiS", 119049 Moscow, Russian Federation*
(Received 27 June 2017; published 18 September 2017)

We analyze the electronic properties of the recently discovered stoichiometric superconductor $CaKFe_4As_4$ by combining an *ab initio* approach and a projection of the band structure to a low-energy tight-binding Hamiltonian, based on the maximally localized Wannier orbitals of the 3*d* Fe states. We identify the key symmetries as well as differences and similarities in the electronic structure between $CaKFe_4As_4$ and the parent systems $CaFe_2As_2$ and KFe_2As_2. In particular, we find $CaKFe_4As_4$ to have a significantly more quasi-two-dimensional electronic structure than the latter systems. Finally, we study the superconducting instabilities in $CaKFe_4As_4$ by employing the leading angular harmonics approximation and find two potential A_{1g}-symmetry representations of the superconducting gap to be the dominant instabilities in this system.

DOI: 10.1103/PhysRevB.96.094521

I. INTRODUCTION

The discovery of the iron-based superconductors (FeSCs) in 2008 created a wide and highly interesting field in solid-state physics [1]. Most of the FeSCs are magnetic metals for the stoichiometric composition and superconduct once the magnetism is destroyed by pressure, disorder, or doping, which results in complex phase diagrams with rich physics [2–4]. The highest T_c is often found at fractional compositions, which due to disorder represents a serious challenge in understanding the pairing mechanism in these systems. In particular, for the nonphononic mechanisms of Cooper pairing, with anisotropic or sign-changing superconducting gaps, any disorder adds extra complications due to a necessity to quantify the pair-breaking effects. Thus, the presence of the few stoichiometric FeSCs offers a unique opportunity to study the phenomenon of superconductivity in these compounds with much higher accuracy both experimentally and theoretically. Among them the recently discovered $CaKFe_4As_4$ (CaK1144) shows a particularly high value of the superconducting transition temperature $T_c \approx 35.8$ K and the upper critical field $H_{c2}^c \approx 71$ T [5–10]. At the same time if one considers the equal ratio of Ca and K in $CaKFe_4As_4$ one could compare this system with hole-doped $Ba_{0.46}K_{0.54}Fe_2As_2$, which has a similar T_c of 34 K [11,12] but is randomly disordered on the single (Ba/K) site.

Overall $CaKFe_4As_4$ is one of the most important representatives of the *AeA*1144 structure family, consisting of alkaline-earth (*Ae*) and alkali (*A*) metals. This structure modifies the intensively studied 122 materials such that the atom in the middle of the unit cell is replaced by an alkali-metal atom [see Fig. 1(a)]. This substitution changes the space group from $I4/mmm$ to the nonsymmetric group $P4/mmm$, since the different *Ae* and *A* layers cause a shift of the intermediate FeAs layer out of their high-symmetry positions. Moreover, in those materials the off positions of the As atoms lead to two different Fe-As distances.

To identify the impact on the superconducting performance, it is necessary to investigate the interplay between crystal and electronic structures in particular stoichiometric iron-based superconductors. To achieve this goal, we investigate the electronic structure of $CaKFe_4As_4$ with *ab initio* methods using density functional theory (DFT). In particular, we systematically compare the electronic structure of the CaK1144 and the KFe_2As_2 and $CaFe_2As_2$(122) materials and analyze doping as well as the influences of the off-symmetry positions of the FeAs layer in $CaKFe_4As_4$. In addition we develop the low-energy description of this system by employing a tight-binding (TB) parametrization of the electronic structure using maximally localized 3*d* Wannier orbitals and discuss the different symmetries within the system. This Hamiltonian will then be used to analyze the superconducting gap function by using the leading angular harmonic approximation (LAHA) method [13–16].

The paper is organized as follows. In Sec. II we present the results of our DFT calculations and compare the electronic properties of CaK1144 and 122 structures. In Sec. III we perform the tight-binding parametrization and discuss the symmetries of the low-energy Hamiltonian. Section IV presents the analysis of the superconducting gap symmetries using LAHA and comparison with the state-of-the-art angle-resolved photoemission spectroscopy (ARPES) data. Finally, we conclude the results of our study in Sec. V.

II. ELECTRONIC STRUCTURE

For the DFT part of our work, we use the Vienna *ab initio* simulation package (VASP) [17–19] with the projector augmented wave [20] basis and employ experimentally obtained crystal parameters for $CaKFe_4As_4$, $CaFe_2As_2$, and KFe_2As_2 as measured previously [5,21,22]. Hereby we use VASP in the generalized gradient approximation [23]. For a better convergence we also consider the *p*-orbital and *s*-orbital states of the Fe and As ions as valence states.

For the tight-binding calculations we use the WANNIER90 package [24] with the in VASP implemented VASP2WANNIER interface, which calculates the maximally localized Wannier functions [25]. Here we focus only on the Fe 3*d* orbitals and neglect the *p* orbitals. Their influence we will discussed later.

In Fig. 2 we present the electronic band structure of $CaKFe_4As_4$ as obtained by DFT. The result is in agreement with previous calculations of Mou *et al.,* where the LDA

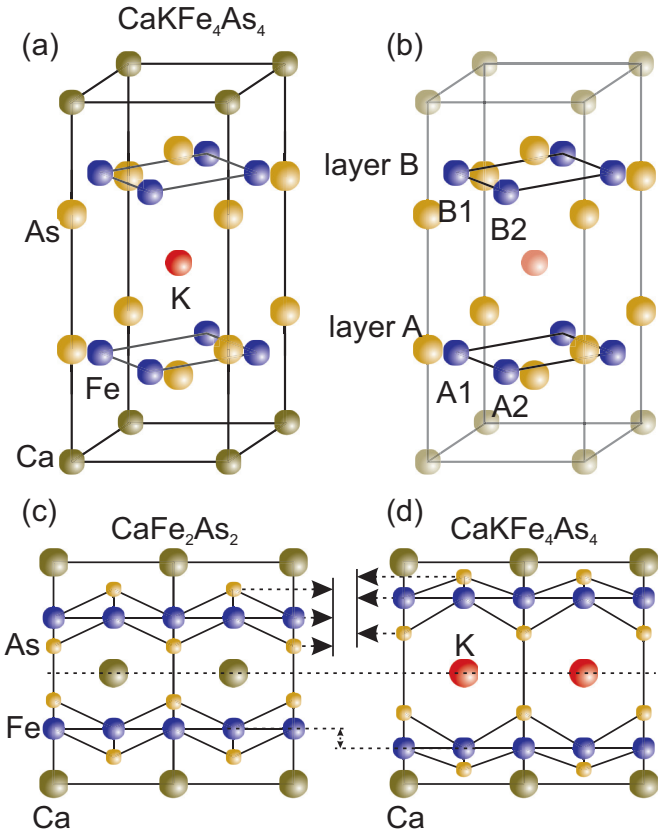

FIG. 1. Atomic structure of $CaKFe_4As_4$ (a) and the definition of the two different FeAs layers (layers A/B) (b). In (c) and (d) the space symmetries of the atom positions of $CaFe_2As_2$ and $CaKFe_4As_4$ are illustrated. For $CaFe_2As_2$ the Fe atoms are in high-symmetry points at $(0, \frac{1}{2}, \pm\frac{1}{4})$ and $(\frac{1}{2}, 0, \pm\frac{1}{4})$. The distance of the As atoms above and below the Fe atoms is equivalent. For $CaKFe_4As_4$ the FeAs layers are shifted away from the high-symmetry points; also the distance of the As atoms is different for the upper and the lower case.

exchange-correlation functional has been used [6]. Note that the degeneracy of bands along the high-symmetry paths $X \to M$ and $R \to A$, which is characteristic for other FeSC [3], is not observable in the present materials. This feature is obviously related to the presence of the Ae and layers surrounding the FeAs layers and the consequent off-symmetry positions of the atoms. In addition, the K atom in $CaKFe_4As_4$ lowers the underlying symmetry of the lattice, which leads to the doubling of the number of electronic bands present in the electronic structure.

From our calculations we find the doping level of the Fe $3d$ shell $n_{\mathrm{CaK1144}} = 5.77$ to lie between the parent stoichiometric 122 materials, since $n_{\mathrm{Ca122}} = 6.07$ and $n_{\mathrm{K122}} = 5.43$. To compare the three systems we have added the letters to Fig. 2 and have performed a rigid band shift for KFe_2As_2 and $CaFe_2As_2$ to acquire the same doping level as $CaKFe_4As_4$. In contrast to $CaKFe_4As_4$, KFe_2As_2 shows a strong three-dimensional (3D) -like behavior of the electronic dispersion along the $\Gamma \to Z$ direction; a strongly dispersive hole pocket is observed. For $CaFe_2As_2$ the dispersion is more two-dimensional (2D) -like than in KFe_2As_2, although the shape of the electron pockets near the M point differs from

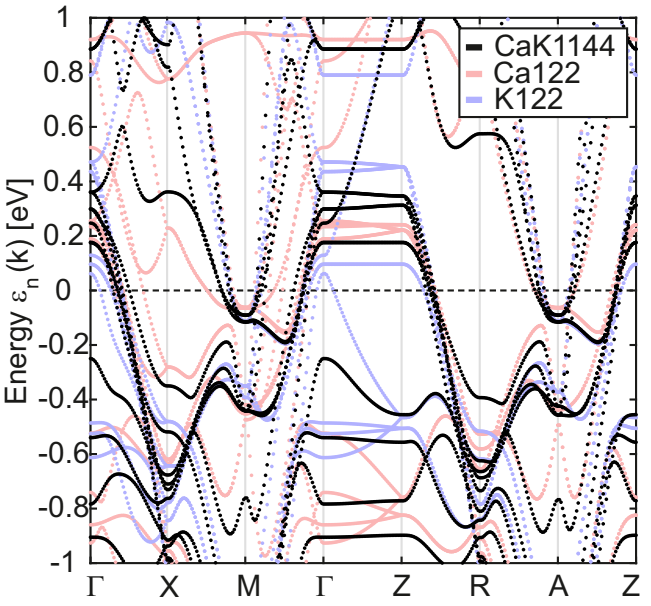

FIG. 2. Electronic dispersion for $CaKFe_4As_4$ (black), $CaFe_2As_2$ (shaded red), and KFe_2As_2 (shaded blue) along the high-symmetry directions of the first Brillouin zone obtained from DFT using experimentally determined lattice parameters [5,21,22]. For better comparison, the electronic structures of $CaFe_2As_2$ and KFe_2As_2 were shifted with a rigid band shift to acquire the same doping level as $CaKFe_4As_4$.

that at the A point, which indicates a significant corrugation of the corresponding cylinder as a function of k_z in $CaFe_2As_2$ as compared to $CaKFe_4As_4$. Thus it seems that $CaKFe_4As_4$ can be considered to be a more 2D-like material with a stronger tendency toward superconductivity as compared to the 122 counterparts.

To make more visible that the structural superposition of $CaFe_2As_2$ and KFe_2As_2 to $CaKFe_4As_4$ is also reflected by the band structure, we present in Fig. 3 the comparison of $CaKFe_4As_4$ electronic band dispersions with those obtained after averaging the electronic dispersions of the $CaFe_2As_2$ and KFe_2As_2 systems. We focus the considerations on the low-energy properties, since they are particularly important for superconductivity. Both structures match rather well except for the features related to the off-symmetry position of the FeAs layers in $CaKFe_4As_4$, namely, the additional splitting of the energy bands at the Γ point of the Brillouin zone (BZ). To see this, observe that compared to the 122 materials

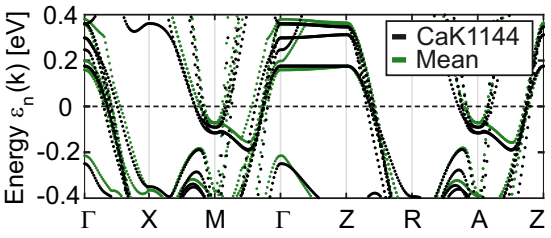

FIG. 3. Electronic dispersion of $CaKFe_4As_4$ (black) compared to the mean of the band energies from $CaFe_2As_2$ and KFe_2As_2 (green).

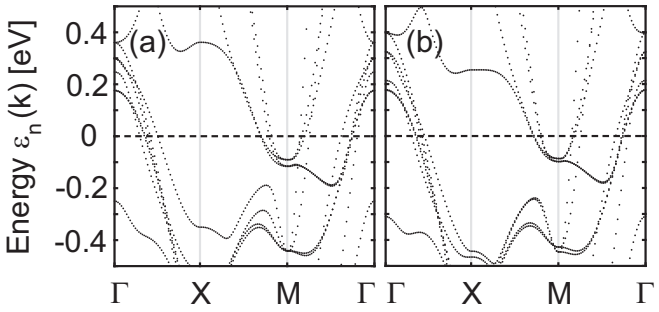

FIG. 4. Influence of the off-symmetry position of the FeAs layers on the electronic band structure of $CaKFe_4As_4$. (a) shows the low-energy part of the electronic dispersion for $CaKFe_4As_4$ using experimental values for the atomic positions, while (b) refers to the electronic dispersion obtained for the high-symmetry Fe positions at $(0,\frac{1}{2},\pm\frac{1}{4})$ and $(\frac{1}{2},0,\pm\frac{1}{4})$. In the latter case, the distance of the As atoms is equivalent in $\pm z$ direction, using $d_{\text{As-Fe}} = 0.105$ Å as the mean of the experimental values.

the FeAs layer of $CaKFe_4As_4$ is nearly 7.3% out of the high-symmetry position at, e.g., $(0,\frac{1}{2},\pm\frac{1}{4})$ [5]. For the band-structure calculations displayed in Fig. 4 the Fe and As atoms are forced to be at the same high-symmetry positions as is the case in 122 materials. Moreover, the two different As atoms are at equivalent positions with respect to the Fe layer. The system is therefore again described by a single Fe-As distance, chosen as the average of the experimental values. The resulting band structure of the high-symmetry artificial structure turns out to be quite similar to the real one except for the slightly different position of the top of the hole bands near the Γ point and larger splitting of the electron bands near the M point of the BZ.

Finally, let us note that similar to the $CaFe_2As_2$ the experimental As positions in $CaKFe_4As_4$ shift by 10% in the process of the relaxation in the nonmagnetic ground state of the DFT calculations. Similar to the recent finding [26], we find the crystal structure is stabilized for the combined state consisting of the $(\pi,0)$ and $(0,\pi)$ ordering wave vectors in the so-called spin-vortex state. However, we are not discussing this further as we are mostly interested in constructing the effective low-energy Hamiltonian to analyze potential superconducting instabilities in $CaKFe_4As_4$ and further employ the experimental positions for the As.

III. TIGHT-BINDING REPRESENTATION

For a better understanding of the electronic correlation in the system, we now construct a TB Hamiltonian for $CaKFe_4As_4$ following the procedure made for other iron-based superconductors [27–29]. For this purpose, we map the orbital-dependent band structure from the DFT calculations on Fe $3d$-orbital Wannier functions using the WANNIER90 package. In Fig. 5 we present the comparison between the orbitally resolved DFT calculations (a) and the tight-binding projection for the band structure (b) in $CaKFe_4As_4$ using the energy window $E_F - 2.2$ eV to $E_F + 3.1$ eV. This corresponds to the best fitting we could achieve. The taken limits cut the different energy bands, such that the p orbitals of the As can be excluded at the lower limit. The energy cutoff is defined by the character of the bands and cannot be strongly varied. In addition, we also set the smaller energy window for the frozen states of ±20 meV near E_F to fit the tight-binding energy bands as accurately as possible. This window is located near the Fermi surface to adequately represent the symmetries of the electronic structure. The corresponding terms of the tight-binding Hamiltonian are given in the Appendix. Observe that the lobes of the $3d$ orbitals are not elongated along the Fe sites [(k_x,k_y) coordinates], such that the orbital content is rotated by 45° in the xy plane, forming (k_1,k_2)-plane coordinates. This, however, does not affect the projection on the Wannier functions. The orbital content observed within DFT is in agreement with the one calculated previously [6]. One of the peculiarities of the $CaKFe_4As_4$ electronic structure is a strong admixture of the d_{z^2} orbital to the states near the Fermi level, which is somewhat different in the $CaFe_2As_2$ and KFe_2As_2 systems.

The tight-binding parametrization using $3d$-Wannier orbitals of the Fe sites, shown in Fig. 5(b), reproduces quite

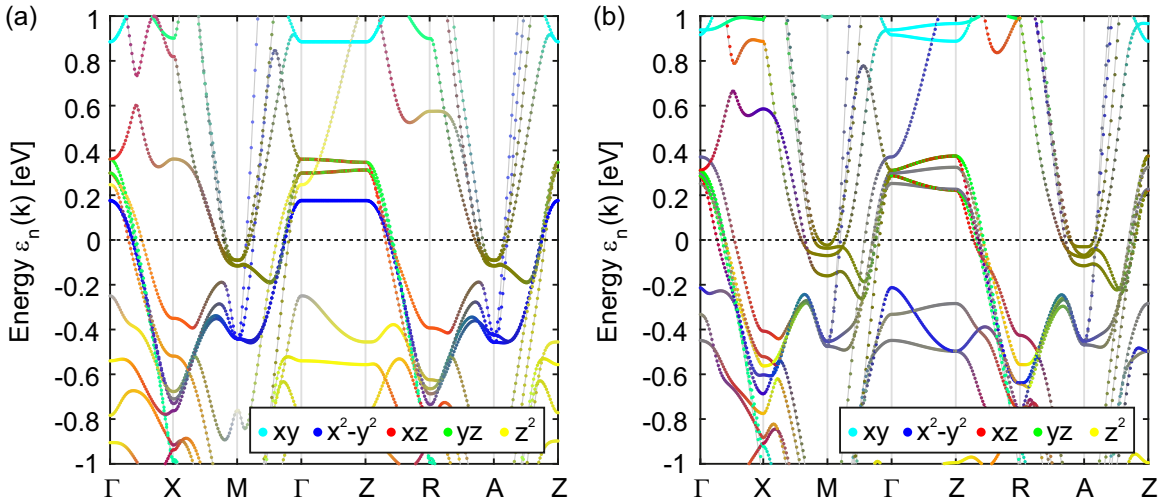

FIG. 5. Comparison between DFT results (a) and the tight-binding (b) parametrization of the energy dispersion and resulting fermiology in $CaKFe_4As_4$. Here, the WANNIER90 evaluation has been restricted to the Fe $3d$-orbital states.

well the electronic structure including the sizes of the electron and hole pockets, their group velocities, and the orbital content. Nevertheless, one can see that for energies outside of a 0.3 eV interval near E_F there are noticeable deviations between DFT and the tight-binding band structures, which are related to the influences of the As p orbitals in this region.

The tight-binding Hamiltonian for $CaKFe_4As_4$ is a good instrument to visualize and estimate the symmetries for this system, which was previously also done for the other Fe-based superconductors [27–29]. Since we limit the TB representation to the $3d$ orbitals, we have only taken the Fe atoms into account. This leads to a block-diagonal form of the Hamiltonian caused by the different positions of the As atoms in typical 122 FeSC material, where one As lies above (+) and another one below (−) the Fe plane. Thus, the Hamiltonian for each FeAs layer acquires the form

$$H_{\mathrm{FeSC}} = \begin{pmatrix} H^{++} & H^{+-} \\ H^{-+} & H^{--} \end{pmatrix}, \tag{1}$$

where the superindices mark the positions of the As atoms. Each block contains five Fe $3d$ orbitals, which leads to the ten orbital-resolved Hamiltonian for typical FeSC. In addition, there are symmetries for the terms in the TB Hamiltonian reflecting the original crystal group symmetry of the lattice in the FeSC:

$$\begin{aligned} H^{++} &= H^{++\dagger}, \quad H^{+-} = H^{+-t}, \\ H^{++} &= H^{--*}, \quad H^{+-} = H^{-+*}. \end{aligned} \tag{2}$$

This reduces the number of necessary TB parameters [27]. With these equations the Hamiltonian gets the form

$$H_{\mathrm{FeSC}} = \begin{pmatrix} H^{++} & H^{+-} \\ H^{+-*} & H^{++*} \end{pmatrix}. \tag{3}$$

For $CaKFe_4As_4$ it is important to take two Fe_2As_2 layers into account due to the specific symmetry of the system [see Figs. 1(b) and 1(d)]. As a result, the Hamiltonian requires a representation with 16 different 5×5 blocks:

$$H_{1144} = \begin{pmatrix} H^{\mathrm{A1A1}} & H^{\mathrm{A1A2}} & H^{\mathrm{A1B1}} & H^{\mathrm{A1B2}} \\ H^{\mathrm{A2A1}} & H^{\mathrm{A2A2}} & H^{\mathrm{A2B1}} & H^{\mathrm{A2B2}} \\ H^{\mathrm{B1A1}} & H^{\mathrm{B1A2}} & H^{\mathrm{B1B1}} & H^{\mathrm{B1B2}} \\ H^{\mathrm{B2A1}} & H^{\mathrm{B2A2}} & H^{\mathrm{B2B1}} & H^{\mathrm{B2B2}} \end{pmatrix}, \tag{4}$$

where A/B refers to the two different Fe_2As_2 layers and the index 1/2 counts the position of the Fe atoms (see Fig. 1). Here, the total Hamiltonian for $CaKFe_4As_4$ can be separated into four blocks, each referring to a given Fe_2As_2 layer:

$$H_{1144} = \begin{pmatrix} H^{\mathrm{AA}} & H^{\mathrm{AB}} \\ H^{\mathrm{BA}} & H^{\mathrm{BB}} \end{pmatrix} = \begin{pmatrix} H^{\mathrm{AA}} & H^{\mathrm{AB}} \\ H^{\mathrm{AB}*} & H^{\mathrm{AA}*} \end{pmatrix}. \tag{5}$$

In the second representation we have utilized the symmetries, shown by Eq. (2), where the +/− index for the above/below As atom has been translated to the A/B index of the FeAs layer within the 1144 family of materials.

Next we look at each particular block within $H^{\mathrm{AA/AB}}$ terms in the Hamiltonian and analyze its symmetry transformations to reduce the number of independent TB parameters. For example, if the system is rotated by 180° around k_2 (R_2) following the initial rotation by 90° around the k_z (R_1) axis the

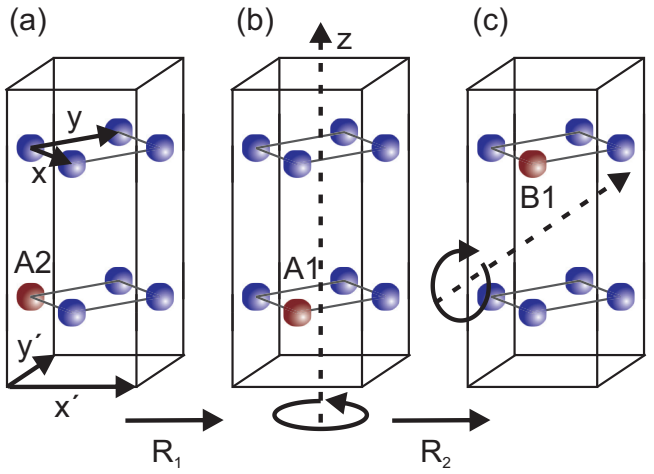

FIG. 6. Introduced symmetry properties of the TB Hamiltonian. The operation R_1 rotates the unit cell by 90° along k_z and R_2 rotates by 180° around the axis, shown on (c). From (a) to (b) the Fe atom A2 is mapped on A1, from (b) to (c) A2 is mapped on B1, thus both Fe_2As_2 layers can be related by this symmetry operation. The arrows x and y refer to the basis vectors in the single Fe unit cell (k_x,k_y in the reciprocal space), while x′ and y′ denote the basis vectors in the 2Fe unit cell (k_1,k_2 in the reciprocal space).

transformed coordinates read

$$\begin{pmatrix} k_1 \\ k_2 \\ k_z \end{pmatrix} \underbrace{\begin{pmatrix} 0 & 1 & 0 \\ -1 & 0 & 0 \\ 0 & 0 & 1 \end{pmatrix}}_{R_1} \underbrace{\begin{pmatrix} -1 & 0 & 0 \\ 0 & 1 & 0 \\ 0 & 0 & -1 \end{pmatrix}}_{R_2} = \begin{pmatrix} k_2 \\ k_1 \\ -k_z \end{pmatrix}. \tag{6}$$

This yields a transformation matrix U in the orbital basis $(d_{xy},d_{x^2-y^2},d_{xz},d_{yz},d_{z^2})$:

$$\underbrace{\begin{pmatrix} 1 & 0 & 0 & 0 & 0 \\ 0 & -1 & 0 & 0 & 0 \\ 0 & 0 & 0 & -1 & 0 \\ 0 & 0 & -1 & 0 & 0 \\ 0 & 0 & 0 & 0 & 1 \end{pmatrix}}_{S} \begin{pmatrix} xy \\ x^2-y^2 \\ xz \\ yz \\ z^2 \end{pmatrix} = \begin{pmatrix} xy \\ -(x^2-y^2) \\ -yz \\ -xz \\ z^2 \end{pmatrix}, \tag{7}$$

characterized by changes in sign and order. In Fig. 6 we illustrate the symmetry transformation H^{A1A1} onto H^{A2A2}, which also can be written as

$$H^{\mathrm{A1A1}}(k_1,k_2,k_z) = S^{-1} H^{\mathrm{A2A2}}(k_2,k_1,-k_z)^* S \tag{8}$$

and H^{B1B1} can be replaced by $H^{\mathrm{A1A1}*}$ according to Eq. (2). Similarly we find

$$\begin{aligned} H^{\mathrm{A1A2}}(k_1,k_2,k_z) &= S^{-1} H^{\mathrm{B2B1}}(k_2,k_1,-k_z) S \\ &= S^{-1} H^{\mathrm{A2A1}}(k_2,k_1,-k_z)^* S. \end{aligned} \tag{9}$$

In addition, there are the symmetry relations

$$H^{\mathrm{A1A1}} = H^{\mathrm{A1A1}*}, \quad H^{\mathrm{A2A1}} = H^{\mathrm{A1A2}\dagger}, \tag{10}$$

which further simplify Eq. (9) to get

$$H^{\mathrm{A1A2}}(k_1,k_2,k_z) = S^{-1} H^{\mathrm{A1A2}}(k_2,k_1,-k_z)^t S. \tag{11}$$

Overall we find for the H^{AB} blocks

$$H^{A2B2}(k_1,k_2,k_z) = S^{-1}H^{A1B1}(k_2,k_1,-k_z)^* S,$$
$$H^{A1B2}(k_1,k_2,k_z) = S^{-1}H^{A1B2}(k_2,k_1,-k_z)^\dagger S, \quad (12)$$

where in the second line we employed

$$H^{A1B1} = H^{A1B1^t}, \quad H^{A2B1} = H^{A1B2^t}, \quad (13)$$

which stems from the symmetry $H^{AB} = H^{AB^t}$. Moreover, the chosen symmetry operations (rotations R_1 and R_2) are necessary to present the tight-binding Hamiltonian in the proper Hermitian form as only the upper triangle of the blocks are sufficient to construct the full Hamiltonian. As a result only four blocks H^{A1A1}, H^{A1A2}, H^{A1B1}, and H^{A1B2} appear now to have an independent form.

Observe that the 122 and 1144 tight-binding Hamiltonians are similar except that the higher symmetry of the 122 systems yields identical hopping matrix elements along the k_1 and k_2 directions [see Eq. (A15) in the Appendix], which is not the case for $CaKFe_4As_4$. Moreover, the hopping for the d_{xz} and d_{yz} orbitals of 122 are interchanged, i.e., $(k_x,k_y) \rightarrow (k_y,k_x)$, except for the sign. The special symmetries of the 122 materials are also present in the hoppings of A1B1 and A1B2. Here, the hoppings along k_z are identical to the hoppings in the (k_1,k_2) plane. This is the result of the gliding symmetry present in 122 and again absent in $CaKFe_4As_4$. Interestingly, this is one of the reasons for the stronger quasi-two-dimensionality in $CaKFe_4As_4$ as compared to the 122 structures. In turn, the quasi-two-dimensional electronic structure allows a relatively straightforward analysis of the superconducting instabilities, which we do in the next section.

IV. HUBBARD-HUND HAMILTONIAN AND SUPERCONDUCTING INSTABILITIES

Based on the single-particle low-energy Hamiltonian, we analyze the superconducting instabilities in $CaKFe_4As_4$ by employing the random phase approximation (RPA) within the LAHA for the Hubbard-Hund Hamiltonian [13,15,16]. This Hamiltonian is given by

$$H_{\rm int} = \frac{U}{2}\sum_{\substack{i,s\\ \sigma}} n_{is\sigma}n_{is\bar{\sigma}} + \frac{U'}{2}\sum_{\substack{i,s\neq t\\ \sigma,\sigma'}} n_{is\sigma}n_{it\sigma'}$$
$$- J\sum_{i,s\neq t} S_{is}\cdot S_{it} + \frac{J'}{2}\sum_{\substack{i,s\neq t\\ \sigma}} d^\dagger_{is\sigma}d^\dagger_{is\bar{\sigma}}d_{it\bar{\sigma}}d_{it\sigma}. \quad (14)$$

where s and t here refer to the orbital indices. The other symbols label the intraorbital Hubbard interaction U, the interorbital Hubbard interaction U', the interorbital exchange J, and the pair hopping term J'. We assume that the interactions originate from a single two-body term with spin rotational invariance, i.e., $J' = J$ and $U' = U - 5J/2$. This leaves U and J as the only two parameters in the problem. Here, U defines the overall magnitude of the pairing interaction, while the structure of the superconducting gap depends on the single parameter J/U, which we will vary.

In order to study the BCS-type superconductivity in the band representation, the interactions need to be rewritten in terms of the band operators. The transformed interactions describe the repulsion between band fermions and acquire a momentum (angular) dependence because of the underlying orbital structure. We use the LAHA formalism to solve the BCS-type gap equation [14–16] by separating each interaction between fermions on the i and j pockets ($i,j = h_1,\ldots,h_6$ and $e_1,\ldots,e_4$) into s-wave, $d_{x^2-y^2}$, and d_{xy} channels. As the superconducting gap symmetry in $CaKFe_4As_4$ belongs to the A_{1g}-symmetry representation [6] we restrict ourselves only to these solutions to make the gap equation tractable semianalytically and to be able to follow the gap evolution upon changing the parameters.

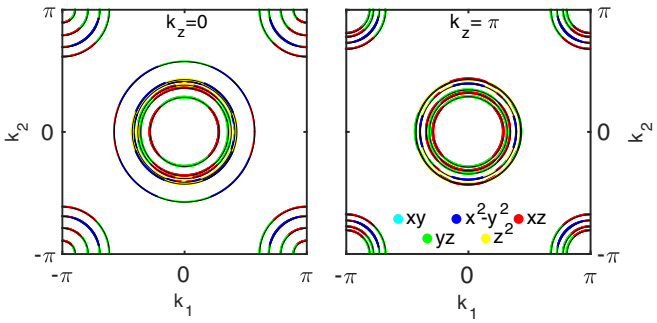

FIG. 7. Fermi surface structure of the $CaKFe_4As_4$ for two different k_z cuts with six hole and four electron Fermi surface pockets. The electronic states at the Fermi level are colored regarding their largest contribution from the iron 3d orbitals.

We apply LAHA, solve for superconductivity, and vary the parameters of the underlying model to see whether the solutions that we find are stable with respect to the variation of the interactions. Choosing this approach, orbital effects and spin fluctuations will determine the strength of the effective interactions that describe the scattering of a Cooper pair between different Fermi surface pockets and will determine the gap structure. We extend the computational procedure described in [13] to the fermiology of Ca1144 to compare possible superconducting s-wave spin-singlet states.

The transformation for the repulsive on-site Coulomb interactions is a consequence of the diagonalization of the kinetic part of the Hamiltonian, which is given in a tight-binding representation (Sec. III). In the notation of [13,15], the effective interactions are named $\Gamma_{ij}(\mathbf{k},\mathbf{k}')$.

Once the problem is reduced to Cooper pairs near the Fermi level, i.e., once the momenta are constrained to the contours of the Fermi surface pockets in the k_x-k_y plane, the momentum dependence can be decomposed into leading angular harmonics. The Fermi surface pockets are quasi-2D cylinders (Fig. 7), which are periodic in the k_z direction. Therefore, it is also possible to find the leading harmonics of the k_z momentum dependence of the effective interactions and the gap function. However, we note that the first harmonic, i.e., a constant, is already a good approximation. In other words, we solve the 3D BCS-type gap equations, but only give the 2D result as first-order approximation, since the gap function is only weakly dispersing in the k_z direction.

Since the Fermi surface topology of $CaKFe_4As_4$ consists of electron and hole pockets of a relatively small radius and shows a weak k_z dispersion, we can apply LAHA, where

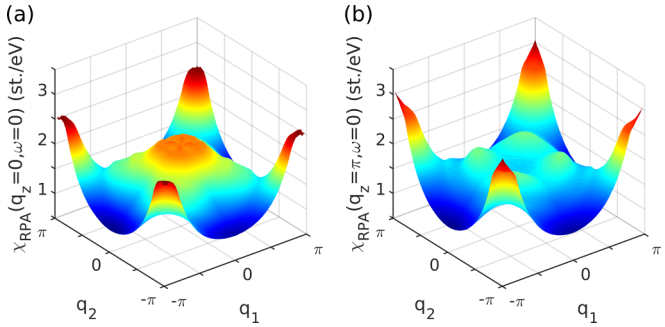

FIG. 8. Multiorbital spin susceptibility within RPA approximation at zero temperature for $q_z = 0$ (a), $q_z = \pi$ (b), Coulomb repulsion $U = 1.5$ eV, and Hund $J = 0.1U$.

the Cooper-pair scattering can be distinguished between the intraband (small $\mathbf{q}$) and interband (large $\mathbf{q}$) ones. Interestingly, in contrast to the situation of some ferropnictides like LiFeAs, where a strong orbital differentiation for some of the pockets takes place, here the orbital character of d_{xz}, $d_{x^2-y^2}$, and d_{yz} is nearly equally distributed between electron and hole pockets, which is also seen in Fig. 5. Furthermore, the hole bands also acquire some d_{z^2} character, which is often also the case in other iron-based superconductors. Its influence was usually ignored in effective models, which consider a d_{xz}, $d_{x^2-y^2}$, and d_{yz} orbital character only [15].

In the next step we compute the spin response functions within RPA, following the original proposal in Ref. [28]. The spectral representation of the Green's function is given as

$$G_{sp}(k,i\omega_n) = \sum_{\mu} \frac{a^s_\mu(k)a^{p*}_\mu(k)}{i\omega_n - E_\mu(k)}. \tag{15}$$

Here, the matrix elements $a^s_\mu(k) = \langle s|\mu k\rangle$ connect the orbital indices s,p and the band index μ and are the components of the eigenvectors resulting from the diagonalization of the tight-binding Hamiltonian. We find the noninteracting susceptibilities

$$\chi^{pq}_{st}(q,\omega) = -\frac{1}{N}\sum_{k,\mu\nu} \frac{a^s_\mu(k)a^{p*}_\mu(k)a^q_\nu(k+q)a^{t*}_\nu(k+q)}{\omega + E_\nu(k+q) - E_\mu(k) + i0^+} \times \{f[E_\nu(k+q)] - f[E_\mu(k)]\}. \tag{16}$$

The RPA expression for the spin susceptibility is given in the form of the Dyson-type equation

$$\left(\chi_1^{\mathrm{RPA}}\right)^{pq}_{st} = \chi^{pq}_{st} + \left(\chi_1^{\mathrm{RPA}}\right)^{pq}_{uv}(U^s)^{uv}_{wz}\chi^{wz}_{st}, \tag{17}$$

where the summation is assumed over repeated indices. Here the nonzero components of the matrices of the spin-dependent interaction U^s are given as

$$(U^s)^{aa}_{aa} = U, \quad (U^s)^{aa}_{bb} = \tfrac{1}{2}J,$$
$$(U^s)^{ab}_{ab} = \tfrac{1}{4}J + U', \quad (U^s)^{ba}_{ab} = J',$$

where $a \neq b$.

The results of the calculations are shown in Fig. 8 for two different k_z cuts. One could clearly see that even for the moderate values of the interaction the susceptibilities are enhanced for the antiferromagnetic wave vector reflecting the nesting of the hole and electron dispersions, $E_e(\mathbf{k}) = -E_h(\mathbf{k}+\mathbf{Q})$ for $\mathbf{Q} = (\pi,\pi)$ in the two Fe BZs. Furthermore, one clearly sees the peaks at smaller wave vectors, resulting from the scattering between the hole bands.

TABLE I. Effective interactions; scattering of Cooper pairs from one hole pocket to another.

Γ_{ij}	h_1	h_2	h_3	h_4	h_5	h_6
h_1	0.61	0.61	0.12	0.08	0.09	0.08
h_2		0.58	0.11	0.06	0.08	0.07
h_3			0.49	0.07	0.32	0.33
h_4				1.10	0.08	0.09
h_5					0.42	0.44
h_6						0.39

The spin fluctuation component of the interaction is obtained by summing up second- and higher-order ladder diagrams in the orbital formalism. The total interaction is then converted from orbital to band basis by dressing it by matrix elements associated with the hybridization of Fe orbitals [13]. Aiming at the analysis of superconductivity, the end result of this procedure is the effective BCS-type Hamiltonian in the band description

$$\mathcal{H} = \sum_{i,\mathbf{k}} \epsilon_i(\mathbf{k})c^\dagger_{i\mathbf{k}}c_{i\mathbf{k}} + \sum_{i,j,\mathbf{k},\mathbf{k}'} \Gamma_{ij}(\mathbf{k},\mathbf{k}')c^\dagger_{i\mathbf{k}}c^\dagger_{i-\mathbf{k}}c_{j\mathbf{k}'}c_{j-\mathbf{k}'}. \tag{18}$$

The quadratic term describes low-energy excitations near hole and electron Fermi surface sheets, labeled by i and j, and the interaction term describes the scattering of a pair $(k\uparrow, -k\downarrow)$ on the pocket i to a pair $(-k'\uparrow, k'\downarrow)$ on the pocket j. The effective singlet interaction $\Gamma_{ij}(\mathbf{k},\mathbf{k}')$ is then given by

$$\Gamma_{ij}(\mathbf{k},\mathbf{k}') = \sum_{s,t,p,q} a^{t*}_{\nu_i}(-\mathbf{k})a^{s*}_{\nu_i}(\mathbf{k})\mathrm{Re}\left[\Gamma^{pq}_{st}(\mathbf{k},\mathbf{k}',0)\right] \times a^p_{\nu_j}(\mathbf{k}')a^q_{\nu_j}(-\mathbf{k}'), \tag{19}$$

with

$$\Gamma^{pq}_{st}(\mathbf{k},\mathbf{k}',\omega) = \left[\tfrac{3}{2}U^s\chi_1^{\mathrm{RPA}}(\mathbf{k}-\mathbf{k}',\omega)U^s + \tfrac{1}{2}U^s\right]^{tq}_{ps}. \tag{20}$$

Here we drop the orbital (charge) -fluctuation contribution as described in Ref. [13].

In Tables I–III we present exemplarily for $U = 1.5$ eV and $J/U = 0.1$ the results of the LAHA projection for the intraband and interband interaction for the ten pockets in $CaKFe_4As_4$. As experimentally the angular variation of the superconducting gap on each pocket is found to be negligible [6] and its global symmetry is consistent with an A_{1g} irreducible symmetry representation, we restrict ourselves

TABLE II. Effective interactions; scattering of Cooper pairs from one electron pocket to another.

Γ_{ij}	e_1	e_2	e_3	e_4
e_1	0.42	0.06	0.30	0.35
e_2		1.08	0.04	0.04
e_3			0.75	0.28
e_4				0.66

TABLE III. Effective interactions; scattering of Cooper pairs from hole pockets to electron pockets.

Γ_{ij}	e_1	e_2	e_3	e_4
h_1	0.87	0.10	0.87	0.46
h_2	0.47	0.19	0.42	0.31
h_3	0.57	0.12	0.53	0.54
h_4	0.42	0.46	0.54	0.33
h_5	0.50	0.68	0.37	0.83
h_6	0.12	1.50	0.10	0.13

to the constant superconducting gaps on each Fermi surface pocket and constant interactions. On average we find that the Cooper-pairing interactions are stronger between electron and hole bands than between bands of the same character, i.e., hole-hole or electron-electron bands, which is a result of the spin fluctuation enhancement of the Cooper-pairing interaction. Nevertheless, there is still strong intraband repulsion for some of the bands such as e_2 or h_4.

We substitute the obtained interactions into the multiband version of the coupled linearized BCS equation, which has the form

$$(-\lambda)\begin{pmatrix}\Delta_{h_1}\\ \vdots\\ \Delta_{h_6}\\ \Delta_{e_1}\\ \vdots\\ \Delta_{e_4}\end{pmatrix} = L\begin{pmatrix}\Gamma_{h_1h_1} & \dots & \Gamma_{h_1h_6} & \Gamma_{h_1e_1} & \dots & \Gamma_{h_1e_4}\\ \vdots & \ddots & \vdots & \vdots & \ddots & \vdots\\ \Gamma_{h_6h_1} & \dots & \Gamma_{h_6h_6} & \Gamma_{h_6e_1} & \dots & \Gamma_{h_6e_4}\\ \Gamma_{e_1h_1} & \dots & \Gamma_{e_1h_6} & \Gamma_{e_1e_1} & \dots & \Gamma_{e_1e_4}\\ \vdots & \ddots & \vdots & \vdots & \ddots & \vdots\\ \Gamma_{e_4h_1} & \dots & \Gamma_{e_4h_6} & \Gamma_{e_4e_1} & \dots & \Gamma_{e_4e_4}\end{pmatrix}\begin{pmatrix}\Delta_{h_1}\\ \vdots\\ \Delta_{h_6}\\ \Delta_{e_1}\\ \vdots\\ \Delta_{e_4}\end{pmatrix}. \tag{21}$$

We solve it numerically for various strengths of the intraorbital on-site Coulomb repulsion U and Hund coupling J, following the original procedure [15]. The resulting phase diagram of the leading instabilities in the A_{1g} channel is shown in Fig. 9. Observe also that once the spin fluctuations, which enhance the interaction between electron and hole bands, are included the $d_{x^2-y^2}$-wave (B_{1g}) and d_{xy}-wave (B_{2g}) symmetry solutions

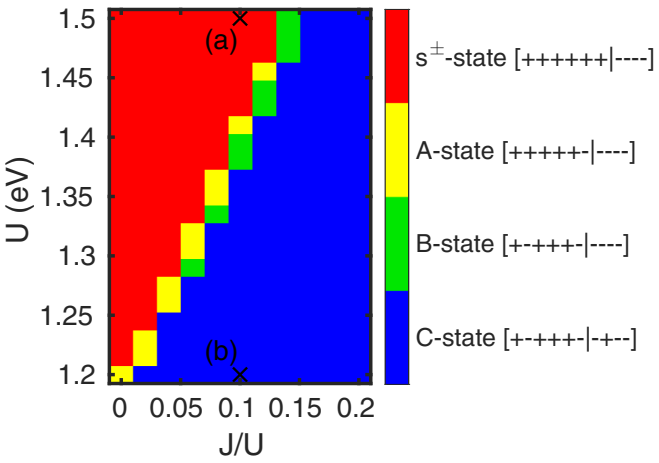

FIG. 9. Sign structure of the leading solution in the A_{1g} channel of the linearized BCS-type gap equations as a function of U and the J/U ratio. The superconducting gap at the six-hole and four-electron Fermi surface pockets can either have a positive or negative sign, which is denoted by the vector $[h_1 \dots h_6, e_1 \dots e_4]$. We find that spin fluctuations at an antiferromagnetic wave vector determine the sign structure of the superconducting gap and lead to a conventional $s^{\pm}$-wave state. In particular, this scenario is likely for $U \gg J$. The crosses refer to the particular ratio of the gaps presented in Fig. 10.

appear to lose against the s-wave ones. Moreover, the angular variation of the gaps within the A_{1g} symmetry representations [i.e., higher harmonics such as $\cos(4\phi)$ on the hole pockets near the Γ point of the BZ] is also quite weak.

As a consequence, the phase diagram is dominated by two types of solutions: The first one could be regarded as a conventional $s^{\pm}$ wave in which the order parameter changes sign between hole and electron pockets. This symmetry is promoted by the strong intraorbital antiferromagnetic spin fluctuations, enhanced by the Coulomb repulsion, U. At the same time, for larger J/U ratios and smaller U the sign structure of the superconducting gaps is distributed in a more sophisticated way between the pockets and involves an additional sign change within the hole and electron pockets. This is mainly due to the fact that for increased J/U ratio some of the interband interactions change sign and become weakly attractive. In addition the spin fluctuation enhancement is weaker for smaller U values. This modifies the balance for the conventional $s^{\pm}$-wave state and promotes states where the order parameter also changes sign within the electron or hole pockets. We obtain the most stable solution of this type, when at least one of the hole and one of the electron pockets changes its sign with respect to their counterparts, which we denote the C-state solutions.

We note that our theory contains more bands than seen in ARPES experiments [6]. This could be partially due to the near degeneracy of some of the hole pockets as well as the electron ones and their similar orbital content, which prevents their straightforward identification in the ARPES experiments. In addition we also find that the electron and hole bands experience the so-called red/blue shift, i.e., their k_F values are smaller than those found in DFT calculations. This is a general feature observed in many FeSCs [30] and is believed to

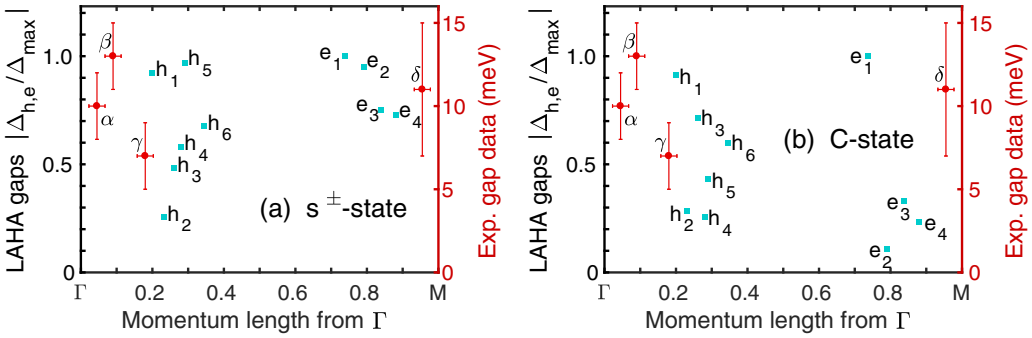

FIG. 10. Mean values of the $s^{\pm}$-wave superconducting gap evaluated on the different Fermi surface pockets for two different values of $U = 1.5$ eV: (a) the conventional $s^{\pm}$ state and $U = 1.2$ eV and (b) the so-called C state and $J/U = 0.1$. The red points refer to experimental values [6].

arise from the effect of the strong interband repulsion between electron and hole bands [31]. Nevertheless, we do not expect that this changes the results of the theoretical calculations as the density of states in two dimensions does not depend on the radius of the Fermi surface sheet, and therefore the interaction strength, determined from LAHA, remains unaffected. In addition we also checked that the orbital character of the bands does not change once the Fermi radius of each of the bands is reduced. Furthermore, the actual value of E_F, counted from the bottom of the electron band, or the top of the hole bands is still much larger than the superconducting gap values, which legitimizes the use of the standard multiband BCS theory. Note that varying slightly the size of the electron and hole pockets will also effectively change the electronic interactions in the band representation and should be equivalent to the change of the initial intra- and interorbital electronic interactions we made to analyze the stability of the A_{1g} symmetry state.

Experimentally, also the sizes of the superconducting gap on some of the Fermi surface sheets, namely, on three hole pockets and one electron pocket, were measured by ARPES [6]. In particular, it was found that the largest gap appears for the electron and hole pockets that are nearly perfectly nested, which was interpreted in favor of the conventional $s^{\pm}$-wave gap. In Fig. 10 we present the results of our calculations from the phase diagram, shown in Fig. 9 for the $s^{\pm}$ wave (a) and the C state (b) that best match the experimental values [6]. We observe that the sizes of the gaps for the $s^{\pm}$-wave states is closer to the values found experimentally. For the C state it turns out that there is a larger distribution of the gaps on the electron Fermi surface cylinders, which would be reflected in the near-nodal behavior of the quasiparticle excitations on some of the electron pockets, which is not seen up to now. The conventional $s^{\pm}$ state shows values which are quite consistent with those found experimentally. This is further supported by the proximity to the nesting of the electron and hole bands. Nevertheless, phase sensitive experiments are needed to confirm this state in $CaKFe_4As_4$.

Unfortunately, the three-dimensional character of the bands in $CaFe_2As_2$ or KFe_2As_2 does not allow an immediate application of the LAHA approach to these 122 systems. However, on general grounds one would expect the stronger tendency toward $s^{\pm}$ superconductivity in $CaKFe_4As_4$ due to the revealed two-dimensional character of the electronic bands in the latter. In principle, we expect that moving the layers in the nonsymmetric position should enhance the two-dimensionality of the system, allowing easier formation of unconventional superconductivity.

V. CONCLUSION

To conclude, we investigated the electronic structure in $CaKFe_4As_4$ using density functional theory. We systematically compared the electronic structure of the 1144 and the 122 materials and analyzed the influences of the off-symmetry positions of the FeAs layer in $CaKFe_4As_4$. In particular, we find that $CaKFe_4As_4$ could be well described as a doped 122 system with some caveat, introduced by the off-symmetry position of the Fe_2As_2 layers in $CaKFe_4As_4$. Among them is a near degeneracy of several hole bands near the Fermi level and their multiple orbital content, consisting of d_{yz}, d_{xz}, d_{xy} ($d_{x^2-y^2}$), and d_{z^2} orbitals. One of the most important consequences, however, is the actual two-dimensional electronic structure in $CaKFe_4As_4$ as compared to 122 materials, which arise due to the absence of the gliding symmetry in $CaKFe_4As_4$.

We develop the low-energy description of this system by projecting the DFT electronic structure on the tight-binding (TB) Hamiltonian based on the Fe $3d$ orbitals only and discuss the different symmetries within the system. We then use this Hamiltonian and Hubbard-Hund intrasite interaction terms as a basis to investigate potential superconducting instabilities in $CaKFe_4As_4$. The nesting between strongly two-dimensional electron and hole bands supports strongly the A_{1g} symmetry representation for the superconducting gap with most likely $s^{\pm}$-wave symmetry where the gap magnitude changes phase between electron and hole pockets. For the increased Hund coupling, J other solutions are also possible and it remains to be determined experimentally which particular phase structure the superconducting order parameter has in $CaKFe_4As_4$.

Note added. After our study was completed, inelastic neutron scattering experiments on $CaKFe_4As_4$ have reported the observation of the so-called neutron spin resonance peak in the superconducting state of this system at the antiferromagnetic wave vector $\mathbf{Q}_{AF} = (\pi,\pi)$ [32]. Most importantly, the position of the spin resonance at $\hbar\Omega_{res} = 12.5$ meV occurs at energies below the smallest sum of the superconducting gaps on the electron and hole pockets ($\hbar\Omega_{res} \leqslant |\Delta_e| + |\Delta_h|$) [6]. This supports the conventional $s^{\pm}$-wave symmetry of the supercon-

ducting gap with gap changing sign between hole and electron pockets and is in full agreement with our theoretical analysis.

ACKNOWLEDGMENTS

We thank R. Valenti, and P. Hirschfeld for discussions. F.A. and I.E. were supported by the joint DFG-ANR Project (ER 463/8-1). I.E. also acknowledges support by the Ministry of Education and Science of the Russian Federation in the framework of Increase Competitiveness Program of NUST MISiS (K2-2016-067).

APPENDIX: TIGHT-BINDING HAMILTONIAN

In this Appendix we present the tight-binding Hamiltonian as obtained with the VASP2WANNIER package. This representation is applicable not only for the 1144 materials, but also for the 122 compounds, which underlines the similarity of both systems. In particular, the elements of Eq. (4) read

$$
\begin{aligned}
H_{11}^{\mathrm{A1A1}} &= t_{11}^{000} + 2t_{11}^{010}\cos k_2 + 2t_{11}^{100}\cos k_1 \\
&\quad + 2t_{11}^{020}\cos(2k_2) + 2t_{11}^{200}\cos(2k_1) \\
&\quad + 4t_{11}^{110}\cos k_1\cos k_2, \\
H_{12}^{\mathrm{A1A1}} &= 4t_{12}^{110}\sin k_1\sin k_2, \\
H_{13}^{\mathrm{A1A1}} &= 2it_{13}^{010}\sin k_2 - 4it_{13}^{110}\cos k_1\sin k_2, \\
H_{14}^{\mathrm{A1A1}} &= 2it_{14}^{100}\sin k_1, \\
H_{15}^{\mathrm{A1A1}} &= 4t_{15}^{110}\sin k_1\sin k_2, \\
H_{22}^{\mathrm{A1A1}} &= t_{22}^{000} + 2t_{22}^{010}\cos k_2 + 2t_{22}^{100}\cos k_1 \\
&\quad + 2t_{22}^{020}\cos(2k_2) + 2t_{22}^{200}\cos(2k_1) \\
&\quad + 4t_{22}^{110}\cos k_1\cos k_2, \\
H_{23}^{\mathrm{A1A1}} &= 2it_{23}^{100}\sin k_1 + 2it_{23}^{200}\sin(2k_1) \\
&\quad + 4it_{23}^{110}\sin k_1\cos k_2 \\
&\quad + 4it_{23}^{210}\sin(2k_1)\cos k_2, \\
H_{24}^{\mathrm{A1A1}} &= 2it_{24}^{010}\sin k_2 + 4it_{24}^{110}\cos k_1\sin k_2 \\
&\quad + 4it_{24}^{120}\cos k_1\sin(2k_2), \qquad \text{(A1)} \\
H_{25}^{\mathrm{A1A1}} &= t_{25}^{000} + 2t_{25}^{010}\cos k_2 + 2t_{25}^{100}\cos k_1 \\
&\quad + 2t_{25}^{020}\cos(2k_2) + 2t_{25}^{200}\cos(2k_1) \\
&\quad + 4t_{25}^{110}\cos k_1\cos k_2, \\
H_{33}^{\mathrm{A1A1}} &= t_{33}^{000} + 2t_{33}^{010}\cos k_2 + 2t_{33}^{100}\cos k_1 \\
&\quad + 2t_{33}^{200}\cos(2k_1) + 4t_{33}^{110}\cos k_1\cos k_2 \\
&\quad + 2t_{33}^{300}\cos(3k_1), \\
H_{34}^{\mathrm{A1A1}} &= 4t_{34}^{110}\sin k_1\sin k_2, \\
H_{35}^{\mathrm{A1A1}} &= 2it_{35}^{100}\sin k_1 + 2it_{35}^{200}\sin(2k_1), \\
H_{44}^{\mathrm{A1A1}} &= t_{44}^{000} + 2t_{44}^{010}\cos k_2 + 2t_{44}^{100}\cos k_1 \\
&\quad + 2t_{44}^{020}\cos(2k_2) + 4t_{44}^{110}\cos k_1\cos k_2 \\
&\quad + 2t_{44}^{030}\cos(3k_2), \\
H_{45}^{\mathrm{A1A1}} &= 2it_{45}^{010}\sin k_2 + 2it_{45}^{020}\sin(2k_2), \\
H_{55}^{\mathrm{A1A1}} &= t_{55}^{000} + 2t_{55}^{010}\cos k_2 + 2t_{55}^{100}\cos k_1 \\
&\quad + 2t_{55}^{020}\cos(2k_2) + 2t_{55}^{200}\cos(2k_1) \\
&\quad + 4t_{55}^{110}\cos k_1\cos k_2
\end{aligned}
$$

and

$$
\begin{aligned}
H_{16}^{\mathrm{A1A2}} &= 2t_{16}^{000}(\cos k_x + \cos k_y), \\
H_{17}^{\mathrm{A1A2}} &= 2t_{17}^{000}(\cos k_x - \cos k_y) \\
&\quad + 2t_{17}^{010}[\cos(2k_x - k_y) - \cos(k_x - 2k_y)] \\
&\quad + 2t_{17}^{100}[-\cos(2k_x + k_y) + \cos(k_x + 2k_y)], \\
H_{18}^{\mathrm{A1A2}} &= 2it_{18}^{000}(\sin k_x - \sin k_y) \\
&\quad + 2it_{18}^{100}[\sin(2k_x + k_y) - \sin(k_x + 2k_y)] \\
&\quad + 2it_{18}^{200}[\sin(3k_x + 2k_y) - \sin(2k_x + 3k_y)], \\
H_{19}^{\mathrm{A1A2}} &= 2it_{19}^{000}(\sin k_x + \sin k_y) \\
&\quad + 2it_{19}^{010}[\sin(2k_x - k_y) - \sin(k_x - 2k_y)] \\
&\quad + 2it_{19}^{020}[\sin(3k_x - 2k_y) - \sin(2k_x - 3k_y)], \\
H_{1,10}^{\mathrm{A1A2}} &= 2t_{1,10}^{000}(-\cos k_x + \cos k_y) \\
&\quad + 2t_{1,10}^{010}[-\cos(2k_x - k_y) + \cos(k_x - 2k_y)] \\
&\quad + 2t_{1,10}^{100}[-\cos(2k_x + k_y) + \cos(k_x + 2k_y)], \\
H_{27}^{\mathrm{A1A2}} &= -2t_{27}^{000}(\cos k_x + \cos k_y) \\
&\quad + 4t_{27}^{010}[\cos(2k_x)\cos k_y + \cos k_x\cos(2k_y)], \\
H_{28}^{\mathrm{A1A2}} &= 2it_{28}^{000}(\sin k_x + \sin k_y) \\
&\quad + 2it_{28}^{010}[\sin(2k_x - k_y) - \sin(k_x - 2k_y)] \\
&\quad + 2it_{28}^{100}[\sin(2k_x + k_y) + \sin(k_x + 2k_y)], \\
H_{29}^{\mathrm{A1A2}} &= 2it_{29}^{000}(-\sin k_x + \sin k_y) \\
&\quad - 2it_{29}^{010}[\sin(2k_x - k_y) + \sin(k_x - 2k_y)] \\
&\quad + 2it_{29}^{100}[-\sin(2k_x + k_y) + \sin(k_x + 2k_y)], \\
H_{2,10}^{\mathrm{A1A2}} &= -2t_{2,10}^{000}(\cos k_x + \cos k_y) \\
&\quad - 2t_{2,10}^{010}[\cos(2k_x - k_y) + \cos(k_x - 2k_y)] \\
&\quad + 2t_{2,10}^{100}[\cos(2k_x + k_y) + \cos(k_x + 2k_y)], \\
H_{38}^{\mathrm{A1A2}} &= -2t_{38}^{000}(\cos k_x + \cos k_y) \\
&\quad + 2t_{38}^{010}[\cos(2k_x - k_y) + \cos(k_x - 2k_y)] \\
&\quad - 2t_{38}^{100}[\cos(2k_x + k_y) + \cos(k_x + 2k_y)], \\
H_{39}^{\mathrm{A1A2}} &= 2t_{39}^{000}(-\cos k_x + \cos k_y) \\
&\quad + 4t_{39}^{010}[\cos(2k_x)\cos k_y - \cos k_x\cos(2k_y)], \\
H_{3,10}^{\mathrm{A1A2}} &= 2it_{3,10}^{000}(\sin k_x + \sin k_y), \\
H_{48}^{\mathrm{A1A2}} &= 2t_{48}^{000}(-\cos k_x + \cos k_y) \\
&\quad + 4t_{48}^{010}[\cos(2k_x)\cos k_y - \cos k_x\cos(2k_y)], \\
H_{49}^{\mathrm{A1A2}} &= -2t_{49}^{000}(\cos k_x + \cos k_y) \\
&\quad - 2t_{49}^{010}[\cos(2k_x - k_y) + \cos(k_x - 2k_y)]
\end{aligned}
$$

$$
\begin{aligned}
&+2t_{49}^{100}[\cos(2k_x+k_y)+\cos(k_x+2k_y)],\\
H_{4,10}^{\mathrm{A1A2}} &= 2it_{4,10}^{000}(-\sin k_x+\sin k_y)\\
&-2it_{4,10}^{010}[\sin(2k_x-k_y)+\sin(k_x-2k_y)],\\
H_{5,10}^{\mathrm{A1A2}} &= 2t_{5,10}^{000}(\cos k_x+\cos k_y)\\
&-4t_{5,10}^{010}[\cos(2k_x)\cos k_y+\cos k_x\cos(2k_y)]\\
&+2t_{5,10}^{110}[\cos(3k_x)+\cos(3k_y)].
\end{aligned}
\tag{A2}
$$

$$
\begin{aligned}
H_{1,11}^{\mathrm{A1B1}} &= t_{1,11}^{000}+2t_{1,11}^{010}\cos k_2+2t_{1,11}^{100}\cos k_1\\
&+4t_{1,11}^{110}\cos k_1\cos k_2,\\
H_{1,12}^{\mathrm{A1B1}} &= 0,\\
H_{1,13}^{\mathrm{A1B1}} &= 2it_{1,13}^{010}\sin k_2,\\
H_{1,14}^{\mathrm{A1B1}} &= 0,\\
H_{1,15}^{\mathrm{A1B1}} &= 0,\\
H_{2,12}^{\mathrm{A1B1}} &= t_{2,12}^{000}+2t_{2,12}^{010}\cos k_2+2t_{2,12}^{100}\cos k_1\\
&+2t_{2,12}^{020}\cos(2k_2),\\
H_{2,13}^{\mathrm{A1B1}} &= 2it_{2,13}^{100}\sin k_1,\\
H_{2,14}^{\mathrm{A1B1}} &= 2it_{2,14}^{010}\sin k_2+4it_{2,14}^{110}\cos k_1\sin k_2,\\
H_{2,15}^{\mathrm{A1B1}} &= t_{2,15}^{000}+2t_{2,15}^{010}\cos k_2+2t_{2,15}^{100}\cos k_1\\
&+2t_{2,15}^{020}\cos(2k_2),\\
H_{3,13}^{\mathrm{A1B1}} &= t_{3,13}^{000}+2t_{3,13}^{010}\cos k_2\\
&+4t_{3,13}^{110}\cos k_1\cos k_2,\\
H_{3,14}^{\mathrm{A1B1}} &= 0,\\
H_{3,15}^{\mathrm{A1B1}} &= 2it_{3,15}^{100}\sin k_1,\\
H_{4,14}^{\mathrm{A1B1}} &= t_{4,14}^{000}+2t_{4,14}^{010}\cos k_2+2t_{4,14}^{100}\cos k_1\\
&+4t_{4,14}^{110}\cos k_1\cos k_2\\
&+4t_{4,14}^{120}\cos k_1\cos(2k_2),\\
H_{4,15}^{\mathrm{A1B1}} &= 4it_{4,15}^{110}\cos k_1\sin k_2,\\
H_{5,15}^{\mathrm{A1B1}} &= t_{5,15}^{000}+2t_{5,15}^{010}\cos k_2+2t_{5,15}^{100}\cos k_1\\
&+2t_{5,15}^{020}\cos(2k_2)+4t_{5,15}^{110}\cos k_1\cos k_2,
\end{aligned}
\tag{A3}
$$

and for the A1B2 block

$$
\begin{aligned}
H_{1,16}^{\mathrm{A1B2}} &= 0,\\
H_{1,17}^{\mathrm{A1B2}} &= 2t_{1,17}^{000}(\cos k_x-\cos k_y),\\
H_{1,18}^{\mathrm{A1B2}} &= 2it_{1,18}^{000}(\sin k_x-\sin k_y)\\
&-2it_{1,18}^{010}[\sin(2k_x-k_y)+\sin(k_x-2k_y)]\\
&+2it_{1,18}^{100}[\sin(2k_x+k_y)-\sin(k_x+2k_y)],\\
H_{1,19}^{\mathrm{A1B2}} &= 0,\\
H_{1,20}^{\mathrm{A1B2}} &= 0,\\
H_{2,17}^{\mathrm{A1B2}} &= 2t_{2,17}^{000}(\cos k_x+\cos k_y),\\
H_{2,18}^{\mathrm{A1B2}} &= -2it_{2,18}^{000}(\sin k_x+\sin k_y)\\
&+2it_{2,18}^{010}[\sin(2k_x-k_y)-\sin(k_x-2k_y)],\\
H_{2,19}^{\mathrm{A1B2}} &= 2it_{2,19}^{000}(-\sin k_x+\sin k_y)\\
&+2it_{2,19}^{010}[\sin(2k_x-k_y)+\sin(k_x-2k_y)],\\
H_{2,20}^{\mathrm{A1B2}} &= 2t_{2,20}^{000}(\cos k_x+\cos k_y)\\
&+2t_{2,20}^{010}[\cos(2k_x-k_y)+\cos(k_x-2k_y)],\\
H_{3,18}^{\mathrm{A1B2}} &= -2t_{3,18}^{000}(\cos k_x+\cos k_y)\\
&+2t_{3,18}^{110}[\cos(3k_x)+\cos(3k_y)],\\
H_{3,19}^{\mathrm{A1B2}} &= 0,\\
H_{3,20}^{\mathrm{A1B2}} &= -2it_{3,20}^{000}(\sin k_x+\sin k_y),\\
H_{4,19}^{\mathrm{A1B2}} &= H_{3,18}^{\mathrm{A1B2}},\\
H_{4,20}^{\mathrm{A1B2}} &= 2it_{4,20}^{000}(\sin k_x-\sin k_y),\\
H_{5,20}^{\mathrm{A1B2}} &= -2t_{5,20}^{000}(\cos k_x+\cos k_y)\\
&+4t_{5,20}^{010}[\cos(2k_x)\cos k_y+\cos k_x\cos(2k_y)].
\end{aligned}
\tag{A4}
$$

The dispersion part involving the k_z direction has for the A1A1 term

$$
H_{22}^{\mathrm{A1A1}} = 2t_{22}^{001}\cos k_z, \tag{A5}
$$

and for the A1B1 term

$$
\begin{aligned}
H_{1,11}^{\mathrm{A1B1}} &= +\big(t_{1,11}^{001}+2t_{1,11}^{011}\cos k_2+2t_{1,11}^{101}\cos k_1\\
&+4t_{1,11}^{111}\cos k_1\cos k_2\big)e^{-ik_z},\\
H_{1,12}^{\mathrm{A1B1}} &= 0,\\
H_{1,13}^{\mathrm{A1B1}} &= 0,\\
H_{1,14}^{\mathrm{A1B1}} &= +2it_{1,14}^{101}\sin k_1\,e^{-ik_z},\\
H_{1,15}^{\mathrm{A1B1}} &= 0,\\
H_{2,12}^{\mathrm{A1B1}} &= +\big(t_{2,12}^{001}+2t_{2,12}^{011}\cos k_2+2t_{2,12}^{101}\cos k_1\\
&+2t_{2,12}^{201}\cos(2k_1)+4t_{2,12}^{111}\cos k_1\cos k_2\big)e^{-ik_z},\\
H_{2,13}^{\mathrm{A1B1}} &= +2it_{2,13}^{101}\sin k_1\,e^{-ik_z},\\
H_{2,14}^{\mathrm{A1B1}} &= 0,\\
H_{2,15}^{\mathrm{A1B1}} &= +\big[t_{2,15}^{001}+2t_{2,15}^{011}\cos k_2+2t_{2,15}^{101}\cos k_1\\
&+2t_{2,15}^{201}\cos(2k_1)\big]e^{-ik_z},\\
H_{3,13}^{\mathrm{A1B1}} &= +\big[t_{3,13}^{001}+2t_{3,13}^{011}\cos k_2+2t_{3,13}^{101}\cos k_1\\
&+4t_{3,13}^{111}\cos k_1\cos k_2+4t_{3,13}^{211}\cos(2k_1)\cos k_2\big]e^{-ik_z},\\
H_{3,14}^{\mathrm{A1B1}} &= 0,\\
H_{3,15}^{\mathrm{A1B1}} &= +\big(2it_{3,15}^{101}\sin k_1-4it_{3,15}^{111}\sin k_1\cos k_2\big)e^{-ik_z},\\
H_{4,14}^{\mathrm{A1B1}} &= +\big(t_{4,14}^{001}+2t_{4,14}^{011}\cos k_2+2t_{4,14}^{101}\cos k_1\\
&+4t_{4,14}^{111}\cos k_1\cos k_2\big)e^{-ik_z},\\
H_{4,15}^{\mathrm{A1B1}} &= +\big(2it_{4,15}^{011}\sin k_2+4it_{4,15}^{111}\cos k_1\sin k_2\big)e^{-ik_z},\\
H_{5,15}^{\mathrm{A1B1}} &= +\big[t_{5,15}^{001}+2t_{5,15}^{011}\cos k_2+2t_{5,15}^{101}\cos k_1\\
&+2t_{5,15}^{201}\cos(2k_1)+4t_{5,15}^{111}\cos k_1\cos k_2\big]e^{-ik_z},
\end{aligned}
\tag{A6}
$$

as well as the A1B2 part

$$
\begin{aligned}
H^{\mathrm{A1B2}}_{1,16} &= 0,\\
H^{\mathrm{A1B2}}_{1,17} &= +2t^{001}_{1,17}(-\cos k_x + \cos k_y)e^{-ik_z},\\
H^{\mathrm{A1B2}}_{1,18} &= 0,\\
H^{\mathrm{A1B2}}_{1,19} &= +\big\{2it^{001}_{1,19}(\sin k_x + \sin k_y)\\
&\quad + 2it^{011}_{1,19}[\sin(2k_x - k_y) - \sin(k_x - 2k_y)]\\
&\quad - 2it^{101}_{1,19}[\sin(2k_x + k_y)\\
&\quad + \sin(k_x + 2k_y)]\big\}e^{-ik_z},\\
H^{\mathrm{A1B2}}_{1,20} &= +2t^{001}_{1,20}(-\cos k_x + \cos k_y)e^{-ik_z},\\
H^{\mathrm{A1B2}}_{2,17} &= +2t^{001}_{2,17}(\cos k_x + \cos k_y)e^{-ik_z},\\
H^{\mathrm{A1B2}}_{2,18} &= +\big\{2it^{001}_{2,18}(\sin k_x + \sin k_y)\\
&\quad - 2it^{101}_{2,18}[\sin(2k_x + k_y)\\
&\quad + \sin(k_x + 2k_y)]\big\}e^{-ik_z},\\
H^{\mathrm{A1B2}}_{2,19} &= +\big\{2it^{001}_{2,19}(\sin k_x - \sin k_y)\\
&\quad + 2it^{101}_{2,19}[-\sin(2k_x + k_y)\\
&\quad + \sin(k_x + 2k_y)]\big\}e^{-ik_z},\\
H^{\mathrm{A1B2}}_{2,20} &= +\big\{2t^{001}_{2,20}(\cos k_x + \cos k_y)\\
&\quad - 2t^{101}_{2,20}[\cos(2k_x + k_y)\\
&\quad + \cos(k_x + 2k_y)]\big\}e^{-ik_z},\\
H^{\mathrm{A1B2}}_{3,18} &= +\big\{-2t^{001}_{3,18}(\cos k_x + \cos k_y)\\
&\quad + 2t^{111}_{3,18}[\cos(3k_x) + \cos(3k_y)]\big\}e^{-ik_z},\\
H^{\mathrm{A1B2}}_{3,19} &= 0,\\
H^{\mathrm{A1B2}}_{3,20} &= +\big\{2it^{001}_{3,20}(\sin k_x + \sin k_y)\\
&\quad + 2it^{011}_{3,20}[-\sin(2k_x - k_y)\\
&\quad + \sin(k_x - 2k_y)]\big\}e^{-ik_z},\\
H^{\mathrm{A1B2}}_{4,19} &= H^{\mathrm{A1B2}}_{3,18},\\
H^{\mathrm{A1B2}}_{4,20} &= +\big\{2it^{001}_{4,20}(-\sin k_x + \sin k_y)\\
&\quad - 2it^{011}_{4,20}[\sin(2k_x - k_y)\\
&\quad + \sin(k_x - 2k_y)]\big\}e^{-ik_z},\\
H^{\mathrm{A1B2}}_{5,20} &= +\big\{-2t^{001}_{5,20}(\cos k_x + \cos k_y)\\
&\quad + 4t^{101}_{5,20}[\cos(2k_x)\cos k_y\\
&\quad + \cos k_x \cos(2k_y)]\big\}e^{-ik_z}.
\end{aligned}
\tag{A7}
$$

Below we give the parameters of the hopping integrals for the $CaKFe_4As_4$ system for the A1A1 term:

$$
\begin{aligned}
&t^{000}_{11} = 0.247\,088, \quad t^{010}_{11} = -0.128\,852,\\
&t^{100}_{11} = -0.015\,027, \quad t^{020}_{11} = 0.019\,461,\\
&t^{200}_{11} = 0.022\,313, \quad t^{110}_{11} = -0.036\,534,\\
&t^{110}_{12} = 0.018\,133, \quad t^{010}_{13} = 0.174\,436,\\
&t^{110}_{13} = 0.010\,374, \quad t^{100}_{14} = -0.126\,588,\\
&t^{110}_{15} = 0.019\,849, \quad t^{000}_{22} = 0.040\,038,\\
&t^{010}_{22} = 0.233\,719, \quad t^{100}_{22} = -0.084\,639,\\
&t^{020}_{22} = -0.041\,893, \quad t^{200}_{22} = 0,\\
&t^{110}_{22} = -0.017\,867, \quad t^{100}_{23} = -0.058\,680,\\
&t^{200}_{23} = -0.028\,825, \quad t^{110}_{23} = 0,\\
&t^{210}_{23} = 0, \quad t^{010}_{24} = 0.141\,905,\\
&t^{110}_{24} = 0, \quad t^{120}_{24} = 0,\\
&t^{000}_{25} = -0.212\,933, \quad t^{010}_{25} = -0.051\,335,\\
&t^{100}_{25} = -0.085\,047, \quad t^{020}_{25} = 0.013\,004,\\
&t^{200}_{25} = 0.016\,189, \quad t^{110}_{25} = -0.013\,983,\\
&t^{000}_{33} = 0.183\,023, \quad t^{010}_{33} = 0.140\,469,\\
&t^{100}_{33} = 0.336\,148 \quad t^{110}_{33} = -0.015\,620,\\
&t^{200}_{33} = 0.077\,006, \quad t^{300}_{33} = 0.022\,415,\\
&t^{110}_{34} = -0.032\,167, \quad t^{100}_{35} = 0.201\,822,\\
&t^{200}_{35} = 0, \quad t^{000}_{44} = 0.147\,106,\\
&t^{010}_{44} = 0.429\,681, \quad t^{100}_{44} = 0.142\,601,\\
&t^{110}_{44} = -0.011\,815, \quad t^{020}_{44} = 0.082\,600,\\
&t^{030}_{44} = 0.021\,224, \quad t^{010}_{45} = -0.078\,445,\\
&t^{020}_{45} = -0.024\,122, \quad t^{000}_{55} = 0.067\,747,\\
&t^{010}_{55} = -0.112\,947, \quad t^{100}_{55} = 0.248\,170,\\
&t^{110}_{55} = -0.024\,991, \quad t^{200}_{55} = -0.043\,234,\\
&t^{020}_{55} = 0
\end{aligned}
\tag{A8}
$$

and A1A2:

$$
\begin{aligned}
&t^{000}_{16} = -0.381\,198, \quad t^{000}_{17} = 0.202\,289,\\
&t^{010}_{17} = 0.018\,080, \quad t^{100}_{17} = 0,\\
&t^{000}_{18} = 0.347\,157, \quad t^{100}_{18} = 0.039\,476,\\
&t^{200}_{18} = 0.011\,114, \quad t^{000}_{19} = 0.254\,869,\\
&t^{010}_{19} = 0.022\,287, \quad t^{020}_{19} = 0.010\,527,\\
&t^{000}_{1,10} = 0.264\,651, \quad t^{010}_{1,10} = 0,\\
&t^{100}_{1,10} = 0.017\,994, \quad t^{000}_{27} = 0.111\,094,\\
&t^{010}_{27} = 0.027\,008, \quad t^{000}_{28} = 0.204\,372,\\
&t^{010}_{28} = 0, \quad t^{100}_{28} = 0,\\
&t^{000}_{29} = 0.081\,707, \quad t^{010}_{29} = 0.021\,110,\\
&t^{100}_{29} = 0, \quad t^{000}_{2,10} = 0.066\,480,\\
&t^{010}_{2,10} = 0, \quad t^{100}_{2,10} = 0.028\,756,\\
&t^{000}_{38} = 0.229\,540, \quad t^{010}_{38} = 0,\\
&t^{100}_{38} = 0.035\,261, \quad t^{000}_{39} = 0.103\,442,\\
&t^{010}_{39} = 0.032\,044, \quad t^{000}_{3,10} = 0.220\,496,
\end{aligned}
$$

$$t_{48}^{000} = 0.167\,758, \quad t_{48}^{010} = 0.019\,836,$$
$$t_{49}^{000} = t_{38}^{000}, \quad t_{49}^{010} = t_{38}^{100},$$
$$t_{49}^{100} = t_{38}^{010}, \quad t_{4,10}^{000} = 0.054\,671,$$
$$t_{4,10}^{010} = 0.021\,606, \quad t_{5,10}^{000} = 0.113\,811,$$
$$t_{5,10}^{010} = 0.029\,265, \quad t_{5,10}^{110} = 0. \tag{A9}$$

The parameters for the A1B1 block read

$$t_{1,11}^{000} = -0.014\,187, \quad t_{1,11}^{010} = 0,$$
$$t_{1,11}^{100} = 0, \quad t_{1,11}^{110} = 0,$$
$$t_{1,13}^{010} = 0, \quad t_{2,12}^{000} = -0.178\,573,$$
$$t_{2,12}^{010} = -0.079\,501, \quad t_{2,12}^{100} = 0,$$
$$t_{2,12}^{020} = 0, \quad t_{2,13}^{100} = -0.011\,803,$$
$$t_{2,14}^{010} = -0.012\,294, \quad t_{2,14}^{110} = 0.010\,139,$$
$$t_{2,15}^{000} = 0.022\,342, \quad t_{2,15}^{010} = 0,$$
$$t_{2,15}^{100} = 0.017\,056, \quad t_{2,15}^{020} = 0, \tag{A10}$$
$$t_{3,13}^{000} = 0.018\,604, \quad t_{3,13}^{010} = 0.010\,938,$$
$$t_{3,13}^{110} = 0, \quad t_{3,15}^{100} = 0,$$
$$t_{4,14}^{000} = 0.022\,463, \quad t_{4,14}^{010} = 0,$$
$$t_{4,14}^{100} = 0, \quad t_{4,14}^{110} = 0,$$
$$t_{4,14}^{120} = 0, \quad t_{4,15}^{110} = 0,$$
$$t_{5,15}^{000} = -0.015\,017, \quad t_{5,15}^{010} = 0,$$
$$t_{5,15}^{100} = -0.011\,221, \quad t_{5,15}^{110} = 0,$$
$$t_{5,15}^{020} = 0$$

and for A1B2

$$t_{1,17}^{000} = 0, \quad t_{1,18}^{000} = 0,$$
$$t_{1,18}^{010} = 0, \quad t_{1,18}^{100} = 0,$$
$$t_{2,17}^{000} = 0.084\,500, \quad t_{2,18}^{000} = 0,$$
$$t_{2,18}^{010} = 0.010\,832, \quad t_{2,19}^{000} = 0,$$
$$t_{2,19}^{010} = 0, \quad t_{2,20}^{000} = 0.015\,346, \tag{A11}$$
$$t_{2,20}^{010} = 0, \quad t_{3,18}^{000} = 0,$$
$$t_{3,18}^{110} = 0, \quad t_{3,20}^{000} = 0,$$
$$t_{4,20}^{000} = 0, \quad t_{5,20}^{000} = 0,$$
$$t_{5,20}^{010} = 0.$$

Similarly, we find parameters A1A1 3D

$$t_{22}^{001} = 0, \tag{A12}$$

A1B1 3D

$$t_{1,11}^{001} = -0.061\,912, \quad t_{1,11}^{011} = -0.014\,910,$$
$$t_{1,11}^{101} = 0.032\,455, \quad t_{1,11}^{111} = 0.013\,021,$$
$$t_{1,14}^{101} = -0.033\,288, \quad t_{2,12}^{001} = -0.040\,849,$$
$$t_{2,12}^{011} = -0.018\,842, \quad t_{2,12}^{101} = 0.021\,234,$$
$$t_{2,12}^{111} = 0.010\,619, \quad t_{2,12}^{201} = 0,$$
$$t_{2,13}^{101} = -0.028\,809, \quad t_{2,15}^{001} = 0.055\,394,$$
$$t_{2,15}^{011} = 0.028\,108, \quad t_{2,15}^{101} = 0.012\,610,$$
$$t_{2,15}^{201} = 0, \quad t_{3,13}^{001} = 0.117\,064,$$
$$t_{3,13}^{011} = -0.014\,458, \quad t_{3,13}^{101} = 0.063\,591,$$
$$t_{3,13}^{111} = -0.017\,604, \quad t_{3,13}^{211} = -0.017\,878,$$
$$t_{3,15}^{101} = 0.027\,871, \quad t_{3,15}^{111} = 0.015\,766,$$
$$t_{4,14}^{001} = 0.077\,263, \quad t_{4,14}^{011} = -0.018\,486,$$
$$t_{4,14}^{101} = 0.034\,123, \quad t_{4,14}^{111} = 0,$$
$$t_{4,15}^{011} = 0.029\,779, \quad t_{4,15}^{111} = 0.011\,809,$$
$$t_{5,15}^{001} = -0.354\,701, \quad t_{5,15}^{011} = 0.021\,342,$$
$$t_{5,15}^{101} = -0.164\,139, \quad t_{5,15}^{111} = 0,$$
$$t_{5,15}^{201} = 0.014\,937, \tag{A13}$$

and parameters A1B2 3D

$$t_{1,17}^{001} = 0.016\,345, \quad t_{1,19}^{001} = 0.049\,462,$$
$$t_{1,19}^{011} = 0.012\,258, \quad t_{1,19}^{101} = 0,$$
$$t_{1,20}^{001} = 0.010\,052, \quad t_{2,17}^{001} = 0.012\,790,$$
$$t_{2,18}^{001} = 0.027\,296, \quad t_{2,18}^{101} = 0,$$
$$t_{2,19}^{001} = 0, \quad t_{2,19}^{101} = 0, \tag{A14}$$
$$t_{2,20}^{001} = 0.028\,421, \quad t_{2,20}^{101} = 0,$$
$$t_{3,18}^{001} = 0.044\,275, \quad t_{3,18}^{111} = 0.010\,797,$$
$$t_{3,20}^{001} = 0, \quad t_{3,20}^{011} = 0.011\,906,$$
$$t_{4,20}^{001} = 0, \quad t_{4,20}^{011} = 0.013\,628,$$
$$t_{5,20}^{001} = 0.167\,859, \quad t_{5,20}^{101} = 0.$$

The same parameters for $CaFe_2As_2$ are as follows. Parameter A1A1:

$$t_{11}^{000} = -0.365\,859, \quad t_{11}^{010} = -0.052\,564,$$
$$t_{11}^{100} = t_{11}^{010}, \quad t_{11}^{110} = -0.019\,398,$$
$$t_{11}^{020} = 0.016\,116, \quad t_{11}^{200} = t_{11}^{020},$$
$$t_{12}^{110} = 0, \quad t_{13}^{010} = 0.120\,333,$$
$$t_{13}^{110} = 0, \quad t_{14}^{100} = -t_{13}^{010},$$
$$t_{15}^{110} = 0.019\,057, \quad t_{22}^{000} = 0.264\,452,$$
$$t_{22}^{010} = 0.161\,138, \quad t_{22}^{100} = t_{22}^{010},$$
$$t_{22}^{110} = 0.013\,436, \quad t_{22}^{020} = -0.040\,903,$$
$$t_{22}^{200} = t_{22}^{020}, \quad t_{23}^{100} = 0.068\,608,$$
$$t_{23}^{110} = 0.013\,523, \quad t_{23}^{210} = -0.011\,030,$$
$$t_{23}^{200} = 0, \quad t_{24}^{010} = t_{23}^{100},$$

$$
\begin{aligned}
&t_{24}^{110} = t_{23}^{110}, \quad t_{24}^{120} = t_{23}^{210},\\
&t_{25}^{000} = 0, \quad t_{25}^{010} = 0.174\,989,\\
&t_{25}^{100} = -t_{25}^{010}, \quad t_{25}^{110} = 0,\\
&t_{25}^{020} = -0.020\,306, \quad t_{25}^{200} = -t_{25}^{020},\\
&t_{33}^{000} = 0.012\,164, \quad t_{33}^{010} = 0.104\,970,\\
&t_{33}^{100} = 0.324\,250, \quad t_{33}^{110} = 0,\\
&t_{33}^{200} = 0.069\,523, \quad t_{33}^{300} = 0.017\,765,\\
&t_{34}^{110} = -0.038\,357, \quad t_{35}^{100} = 0.151\,463,\\
&t_{35}^{200} = 0.031\,583, \quad t_{44}^{000} = t_{33}^{000},\\
&t_{44}^{010} = t_{33}^{100}, \quad t_{44}^{100} = t_{33}^{010},\\
&t_{44}^{110} = 0, \quad t_{44}^{020} = t_{33}^{200},\\
&t_{44}^{030} = t_{33}^{300}, \quad t_{45}^{010} = -t_{35}^{100},\\
&t_{45}^{020} = -t_{35}^{200}, \quad t_{55}^{000} = -0.089\,032,\\
&t_{55}^{010} = 0, \quad t_{55}^{100} = 0,\\
&t_{55}^{110} = -0.033\,271, \quad t_{55}^{020} = -0.015\,254,\\
&t_{55}^{200} = t_{55}^{020}.
\end{aligned}
\tag{A15}
$$

Parameter A1A2:

$$
\begin{aligned}
&t_{16}^{000} = -0.363\,661, \quad t_{17}^{000} = 0,\\
&t_{17}^{010} = 0.010\,562, \quad t_{17}^{100} = t_{17}^{010},\\
&t_{18}^{000} = 0.244\,647, \quad t_{18}^{100} = 0.022\,411,\\
&t_{18}^{200} = 0, \quad t_{19}^{000} = t_{18}^{000},\\
&t_{19}^{010} = t_{18}^{100}, \quad t_{19}^{020} = t_{18}^{200},\\
&t_{1,10}^{000} = 0.304\,047, \quad t_{1,10}^{010} = 0.011\,386,\\
&t_{1,10}^{100} = t_{1,10}^{010}, \quad t_{27}^{000} = 0.211\,970,\\
&t_{27}^{010} = 0.035\,072, \quad t_{28}^{000} = 0.154\,401,\\
&t_{28}^{010} = 0.014\,769, \quad t_{28}^{100} = 0.021\,142,\\
&t_{29}^{000} = t_{28}^{000}, \quad t_{29}^{010} = t_{28}^{100},\\
&t_{29}^{100} = t_{28}^{010}, \quad t_{2,10}^{000} = 0,\\
&t_{2,10}^{010} = 0.019\,052, \quad t_{2,10}^{100} = t_{2,10}^{010},\\
&t_{38}^{000} = 0.183\,874, \quad t_{38}^{010} = 0.011\,643,\\
&t_{38}^{100} = 0.041\,421, \quad t_{39}^{000} = 0.113\,111,\\
&t_{39}^{010} = 0.023\,085, \quad t_{3,10}^{000} = 0.092\,244,\\
&t_{48}^{000} = t_{39}^{000}, \quad t_{48}^{010} = t_{39}^{010},\\
&t_{49}^{000} = t_{38}^{000}, \quad t_{49}^{010} = t_{38}^{100},\\
&t_{49}^{100} = t_{38}^{010}, \quad t_{4,10}^{000} = -t_{3,10}^{000},\\
&t_{4,10}^{010} = 0, \quad t_{5,10}^{000} = 0.059\,586,\\
&t_{5,10}^{010} = 0.024\,878, \quad t_{5,10}^{110} = 0.013\,588.
\end{aligned}
\tag{A16}
$$

Parameter A1B1:

$$
\begin{aligned}
&t_{1,11}^{000} = -0.062\,812, \quad t_{1,11}^{010} = 0.035\,863,\\
&t_{1,11}^{100} = -0.018\,856, \quad t_{11}^{110} = 0.016\,659,\\
&t_{1,13}^{010} = 0.030\,549, \quad t_{2,12}^{000} = -0.262\,053,\\
&t_{2,12}^{010} = -0.072\,906, \quad t_{2,12}^{100} = -0.025107,\\
&t_{2,12}^{020} = 0.010\,635, \quad t_{2,13}^{100} = 0,\\
&t_{2,14}^{010} = -0.056\,892, \quad t_{2,14}^{110} = 0,\\
&t_{2,15}^{000} = -0.170\,028, \quad t_{2,15}^{010} = -0.090\,345,\\
&t_{2,15}^{100} = 0.031\,744, \quad t_{2,15}^{020} = 0.012\,453,\\
&t_{3,13}^{000} = 0.068\,646, \quad t_{3,13}^{010} = 0.045\,685,\\
&t_{3,13}^{110} = -0.011\,647, \quad t_{3,15}^{100} = -0.018\,612,\\
&t_{4,14}^{000} = 0.110\,209, \quad t_{4,14}^{010} = 0.059\,951,\\
&t_{4,14}^{100} = -0.016\,171, \quad t_{4,14}^{110} = -0.018\,985,\\
&t_{4,14}^{120} = -0.016\,778, \quad t_{4,15}^{110} = 0.020\,444,\\
&t_{5,15}^{000} = -0.156\,738, \quad t_{5,15}^{010} = -0.062\,072,\\
&t_{5,15}^{100} = 0.037\,088, \quad t_{5,15}^{110} = 0.021\,684,\\
&t_{5,15}^{020} = 0.010\,814.
\end{aligned}
\tag{A17}
$$

Parameter A1B2:

$$
\begin{aligned}
&t_{1,17}^{000} = 0.020\,947, \quad t_{1,18}^{000} = 0.051\,860,\\
&t_{1,18}^{010} = 0.011\,344, \quad t_{1,18}^{100} = 0.012\,005,\\
&t_{2,17}^{000} = 0.119\,800, \quad t_{2,18}^{000} = 0.022\,801,\\
&t_{2,18}^{010} = 0.014\,765, \quad t_{2,19}^{000} = 0.030\,462,\\
&t_{2,19}^{010} = 0.012\,601, \quad t_{2,20}^{000} = -0.083\,382,\\
&t_{2,20}^{010} = 0.011\,417, \quad t_{3,18}^{000} = 0.045\,360,\\
&t_{3,18}^{110} = 0.011\,536, \quad t_{3,20}^{000} = 0.023\,115,\\
&t_{4,20}^{000} = 0.011\,132, \quad t_{5,20}^{000} = 0.072\,867,\\
&t_{5,20}^{010} = 0.010\,693.
\end{aligned}
\tag{A18}
$$

Parameter A1A1 3D:

$$
t_{22}^{001} = 0.016\,488. \tag{A19}
$$

Parameter A1B1 3D:

$$
\begin{aligned}
&t_{1,11}^{001} = t_{1,11}^{000}, \quad t_{1,11}^{011} = t_{1,11}^{100},\\
&t_{1,11}^{101} = t_{1,11}^{010}, \quad t_{1,11}^{111} = t_{1,11}^{110},\\
&t_{1,14}^{101} = -t_{1,13}^{010}, \quad t_{2,12}^{001} = t_{2,12}^{000},\\
&t_{2,12}^{011} = t_{2,12}^{100}, \quad t_{2,12}^{101} = t_{2,12}^{010},\\
&t_{2,12}^{111} = 0, \quad t_{2,12}^{201} = t_{2,12}^{020},\\
&t_{2,13}^{101} = t_{2,14}^{010}, \quad t_{2,15}^{001} = -t_{2,15}^{000},\\
&t_{2,15}^{011} = -t_{2,15}^{100}, \quad t_{2,15}^{101} = -t_{2,15}^{010},\\
&t_{2,15}^{201} = -t_{2,15}^{020}, \quad t_{3,13}^{001} = t_{4,14}^{000},
\end{aligned}
$$

$$
\begin{aligned}
&t^{011}_{3,13} = t^{100}_{4,14}, \quad t^{101}_{3,13} = t^{010}_{4,14},\\
&t^{111}_{3,13} = t^{110}_{4,14}, \quad t^{211}_{3,13} = t^{120}_{4,14},\\
&t^{101}_{3,15} = 0, \quad t^{110}_{3,15} = t^{110}_{4,15},\\
&t^{001}_{4,14} = t^{000}_{3,13}, \quad t^{011}_{4,14} = 0,\\
&t^{101}_{4,14} = t^{010}_{3,13}, \quad t^{111}_{4,14} = t^{110}_{3,13},\\
&t^{011}_{4,15} = -t^{100}_{3,15}, \quad t^{111}_{4,15} = 0,\\
&t^{001}_{5,15} = t^{000}_{5,15}, \quad t^{011}_{5,15} = t^{100}_{5,15},\\
&t^{101}_{5,15} = t^{010}_{5,15}, \quad t^{111}_{5,15} = t^{110}_{5,15},\\
&t^{201}_{5,15} = t^{020}_{5,15}.
\end{aligned}
\tag{A20}
$$

Parameter A1B2 3D:

$$
\begin{aligned}
&t^{001}_{1,17} = t^{000}_{1,17}, \quad t^{001}_{1,19} = t^{000}_{1,18}, \quad t^{011}_{1,19} = t^{100}_{1,18}, \quad t^{101}_{1,19} = t^{010}_{1,18},\\
&t^{001}_{1,20} = 0, \quad t^{001}_{2,17} = t^{000}_{2,17}, \quad t^{001}_{2,18} = t^{000}_{2,19}, \quad t^{101}_{2,18} = t^{010}_{2,19},\\
&t^{001}_{2,19} = t^{000}_{2,18}, \quad t^{101}_{2,19} = t^{010}_{2,18},\\
&t^{001}_{2,20} = -t^{000}_{2,20}, \quad t^{101}_{2,20} = t^{010}_{2,20},\\
&t^{001}_{3,18} = t^{000}_{3,18}, \quad t^{111}_{3,18} = t^{110}_{3,18},\\
&t^{001}_{3,20} = t^{000}_{3,20}, \quad t^{011}_{3,20} = 0,\\
&t^{001}_{4,20} = t^{000}_{3,20}, \quad t^{011}_{4,20} = 0,\\
&t^{001}_{5,20} = t^{000}_{5,20}, \quad t^{101}_{5,20} = t^{010}_{5,20}.
\end{aligned}
\tag{A21}
$$

[1] Y. Kamihara, T. Watanabe, M. Hirano, and H. Hosono, J. Am. Chem. Soc. **130**, 3296 (2008).
[2] D. C. Johnston, Adv. Phys. **59**, 803 (2010).
[3] P. Hirschfeld, C. R. Phys. **17**, 197 (2016).
[4] A. V. Chubukov, Annu. Rev. Condens. Matter Phys. **3**, 57 (2012).
[5] A. Iyo, K. Kawashima, T. Kinjo, T. Nishio, S. Ishida, H. Fujihisa, Y. Gotoh, K. Kihou, H. Eisaki, and Y. Yoshida, J. Am. Chem. Soc. **138**, 3410 (2016).
[6] D. Mou, T. Kong, W. R. Meier, F. Lochner, L.-L. Wang, Q. Lin, Y. Wu, S. L. Bud'ko, I. Eremin, D. D. Johnson, P. C. Canfield, and A. Kaminski, Phys. Rev. Lett. **117**, 277001 (2016).
[7] R. Yang, Y. Dai, B. Xu, W. Zhang, Z. Qiu, Q. Sui, C. C. Homes, and X. Qiu, Phys. Rev. B **95**, 064506 (2017).
[8] K. Cho, A. Fente, S. Teknowijoyo, M. A. Tanatar, K. R. Joshi, N. M. Nusran, T. Kong, W. R. Meier, U. Kaluarachchi, I. Guillamón, H. Suderow, S. L. Bud'ko, P. C. Canfield, and R. Prozorov, Phys. Rev. B **95**, 100502(R) (2017).
[9] X. Shi and G. Wang, J. Phys. Soc. Jpn. **85**, 124714 (2016).
[10] W. R. Meier, T. Kong, U. S. Kaluarachchi, V. Taufour, N. H. Jo, G. Drachuck, A. E. Böhmer, S. M. Saunders, A. Sapkota, A. Kreyssig, M. A. Tanatar, R. Prozorov, A. I. Goldman, F. F. Balakirev, A. Gurevich, S. L. Bud'ko, and P. C. Canfield, Phys. Rev. B **94**, 064501 (2016).
[11] Y. Liu, M. A. Tanatar, W. E. Straszheim, B. Jensen, K. W. Dennis, R. W. McCallum, V. G. Kogan, R. Prozorov, and T. A. Lograsso, Phys. Rev. B **89**, 134504 (2014).
[12] K. Cho, M. Kończykowski, S. Teknowijoyo, M. A. Tanatar, Y. Liu, T. A. Lograsso, W. E. Straszheim, V. Mishra, S. Maiti, P. J. Hirschfeld, and R. Prozorov, Sci. Adv. **2**, e1600807 (2016).
[13] S. Maiti, M. M. Korshunov, T. A. Maier, P. J. Hirschfeld, and A. V. Chubukov, Phys. Rev. Lett. **107**, 147002 (2011).
[14] S. Maiti, M. M. Korshunov, T. A. Maier, P. J. Hirschfeld, and A. V. Chubukov, Phys. Rev. B **84**, 224505 (2011).
[15] F. Ahn, I. Eremin, J. Knolle, V. B. Zabolotnyy, S. V. Borisenko, B. Büchner, and A. V. Chubukov, Phys. Rev. B **89**, 144513 (2014).
[16] S. Maiti, M. M. Korshunov, and A. V. Chubukov, Phys. Rev. B **85**, 014511 (2012).
[17] G. Kresse and J. Hafner, Phys. Rev. B **47**, 558 (1993).
[18] G. Kresse and J. Furthmüller, Comput. Mater. Sci. **6**, 15 (1996).
[19] G. Kresse and J. Furthmüller, Phys. Rev. B **54**, 11169 (1996).
[20] P. E. Blöchl, Phys. Rev. B **50**, 17953 (1994).
[21] S. Rózsa and H.-U. Schuster, Z. Naturforsch. B **36**, 1668 (1981).
[22] A. Kreyssig, M. A. Green, Y. Lee, G. D. Samolyuk, P. Zajdel, J. W. Lynn, S. L. Bud'ko, M. S. Torikachvili, N. Ni, S. Nandi, J. B. Leão, S. J. Poulton, D. N. Argyriou, B. N. Harmon, R. J. McQueeney, P. C. Canfield, and A. I. Goldman, Phys. Rev. B **78**, 184517 (2008).
[23] J. P. Perdew, K. Burke, and M. Ernzerhof, Phys. Rev. Lett. **77**, 3865 (1996).
[24] A. A. Mostofi, J. R. Yates, G. Pizzi, Y.-S. Lee, I. Souza, D. Vanderbilt, and N. Marzari, Comput. Phys. Commun. **185**, 2309 (2014).
[25] N. Marzari and D. Vanderbilt, Phys. Rev. B **56**, 12847 (1997).
[26] W. Meier, Q.-P. Ding, A. Kreyssig, S. L. Bud'ko, A. Sapkota, K. Kothapalli, V. Borisov, R. Valentí, C. D. Batista, P. P. Orth, R. M. Fernandes, A. I. Goldman, Y. Furukawa, A. E. Böhmer, and P. C. Canfield, arXiv:1706.01067.
[27] H. Eschrig and K. Koepernik, Phys. Rev. B **80**, 104503 (2009).
[28] S. Graser, T. A. Maier, P. J. Hirschfeld, and D. J. Scalapino, New J. Phys. **11**, 025016 (2009).
[29] H. Ikeda, R. Arita, and J. Kuneš, Phys. Rev. B **81**, 054502 (2010).
[30] A. Charnukha, D. Evtushinsky, C. Matt, N. Xu, M. Shi, B. Büchner, N. D. Zhigadlo, B. Batlogg, and S. Borisenko, Sci. Rep. **5**, 18273 (2015).
[31] L. Ortenzi, E. Cappelluti, L. Benfatto, and L. Pietronero, Phys. Rev. Lett. **103**, 046404 (2009).
[32] K. Iida, M. Ishikado, Y. Nagai, H. Yoshida, A. D. Christianson, N. Murai, K. Kawashima, Y. Yoshida, H. Eisaki, and A. Iyo, J. Phys. Soc. Jpn. **86**, 093703 (2017).